Supplementary information

Enhancement of thermoelectric power factor by tuning the carrier concentration in Cu-rich and Ge-poor colusites $Cu_{26+x}Nb_2Ge_{6-x}S_{32}$

Yohan Bouyrie,[1,†] Raju Chetty,[1,†] Koichiro Suekuni,[2] Noriyuki Saitou,[3] Priyanka Jood,[1,4] Noriko Yoshizawa,[3] Toshiro Takabatake,[5] and Michihiro Ohta[1,4,*]

*Corresponding Author; Email: ohta.michihiro@aist.go.jp

†These authors contributed equally to this work.

1. Research Institute for Energy Conservation, National Institute of Advanced Industrial Science and Technology (AIST), Tsukuba, Ibaraki 305-8568, Japan.

2. Department of Applied Science for Electronics and Materials, Interdisciplinary Graduate School of Engineering Sciences, Kyushu University, Kasuga, Fukuoka 816-8580, Japan.

3. Research Institute of Energy Frontier, National Institute of Advanced Industrial Science and Technology (AIST), Tsukuba, Ibaraki 305-8569, Japan.

4. Global Zero Emission Research Center, National Institute of Advanced Industrial Science and Technology (AIST), Tsukuba, Ibaraki 305-8568, Japan.

5. Graduate School of Advanced Sciences of Matter, Hiroshima University, Higashi-Hiroshima, Hiroshima 739-8530, Japan.

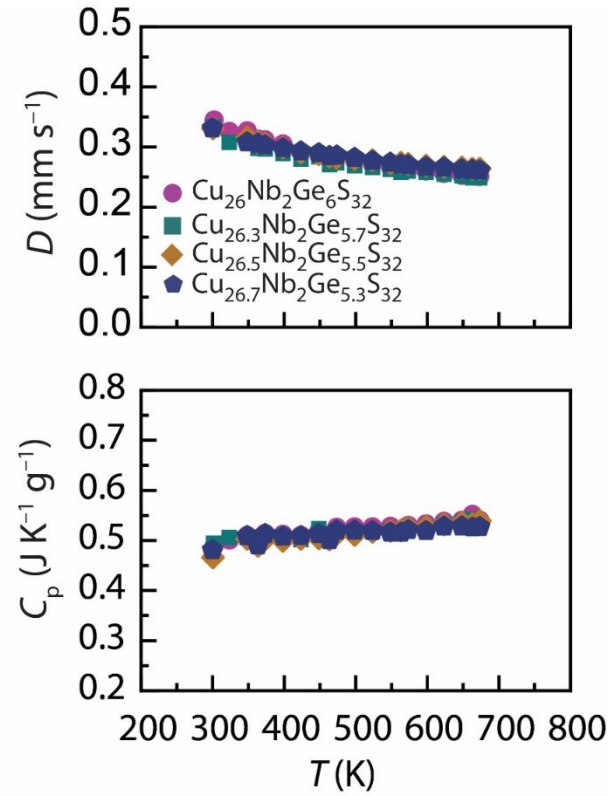

Figure S1

Temperature dependence of the (a) thermal diffusivity D and (b) heat capacity C_p for the sintered compacts of $Cu_{26+x}Nb_2Ge_{6-x}S_{32}$ (x = 0, 0.3, 0.5, 0.7).

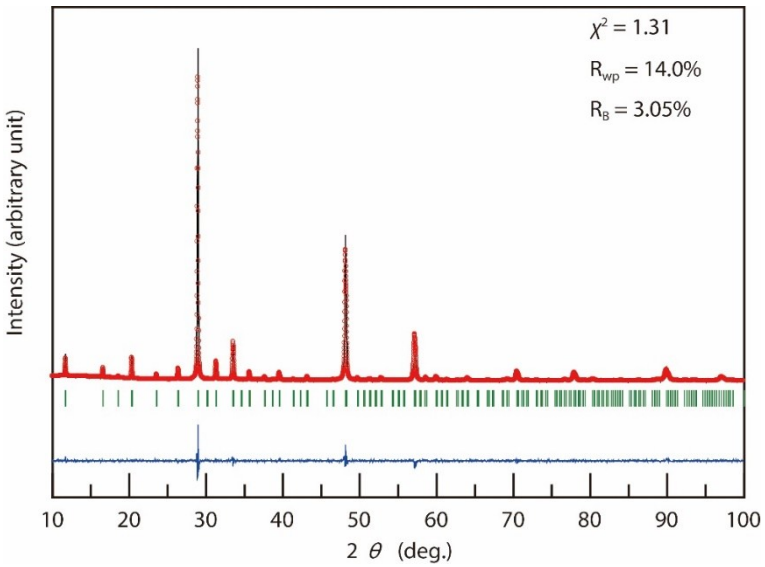

Figure S2

Rietveld refinement of the XRD pattern of the sintered compact of $Cu_{26}Nb_2Ge_6S_{32}$. The experimental data are marked as red dots. The calculated pattern is in black and the difference between experimental and calculated patterns is shown in blue. The vertical green bars stand for the expected Bragg positions of colusite.

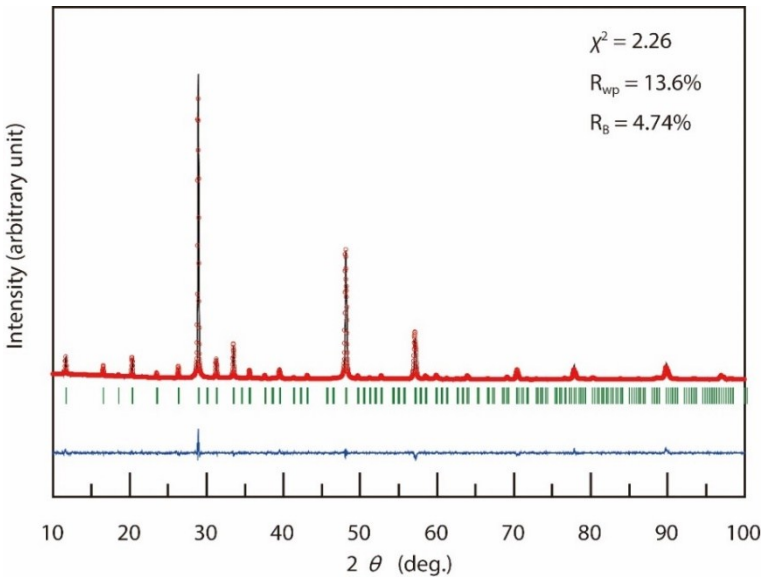

Figure S3

Rietveld refinement of the XRD pattern of the sintered compact of $Cu_{26.3}Nb_2Ge_{5.7}S_{32}$. The experimental data are marked as red dots. The calculated pattern is in black and the difference between experimental and calculated patterns is shown in blue. The vertical green bars stand for the expected Bragg positions of colusite.

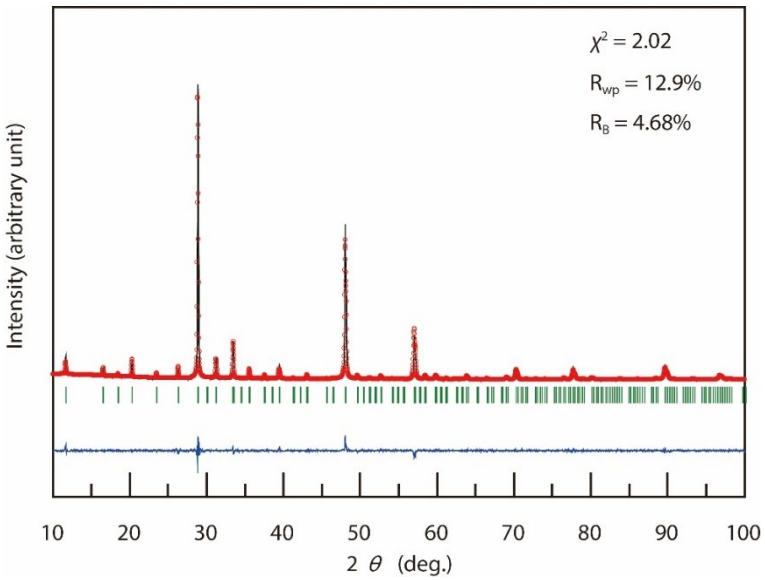

Figure S4

Rietveld refinement of the XRD pattern of the sintered compact of $Cu_{26.5}Nb_2Ge_{5.5}S_{32}$. The experimental data are marked as red dots. The calculated pattern is in black and the difference between experimental and calculated patterns is shown in blue. The vertical green bars stand for the expected Bragg positions of colusite.

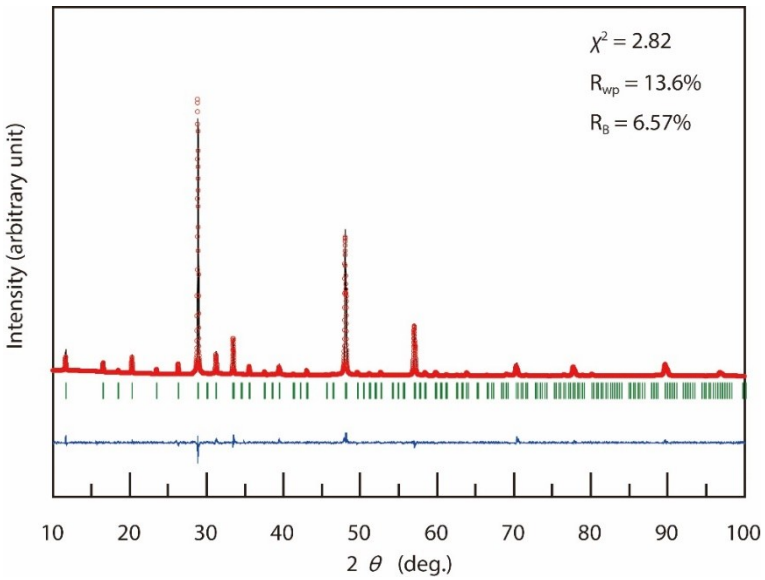

Figure S5

Rietveld refinement of the XRD pattern of the sintered compact of $Cu_{26.7}Nb_2Ge_{5.3}S_{32}$. The experimental data are marked as red dots. The calculated pattern is in black and the difference between experimental and calculated patterns is shown in blue. The vertical green bars stand for the expected Bragg positions of colusite.

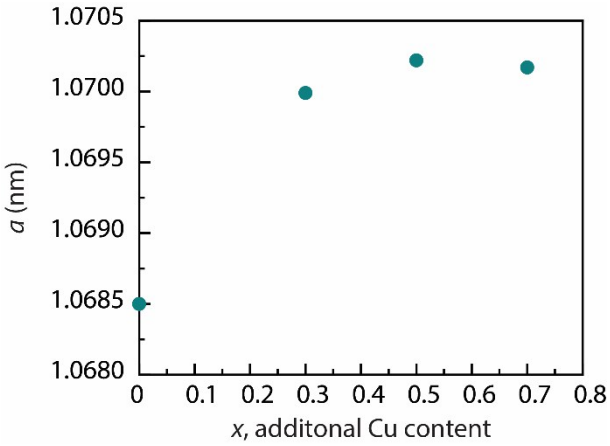

Figure S6

Lattice parameter (*a*) as a function of additional Cu content *x* in $Cu_{26+x}Nb_2Ge_{6-x}S_{32}$.

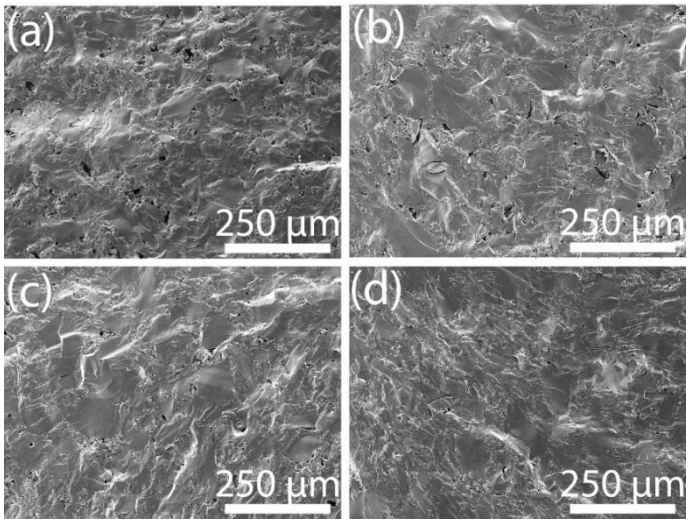

Figure S7

Scanning electron microscopy-secondary electrons images of the fractured surface of the sintered compacts of (a) $Cu_{26}Nb_2Ge_6S_{32}$, (b) $Cu_{26.3}Nb_2Ge_{5.7}S_{32}$, (c) $Cu_{26.5}Nb_2Ge_{5.5}S_{32}$, and (d) $Cu_{26.7}Nb_2Ge_{5.3}S_{32}$.

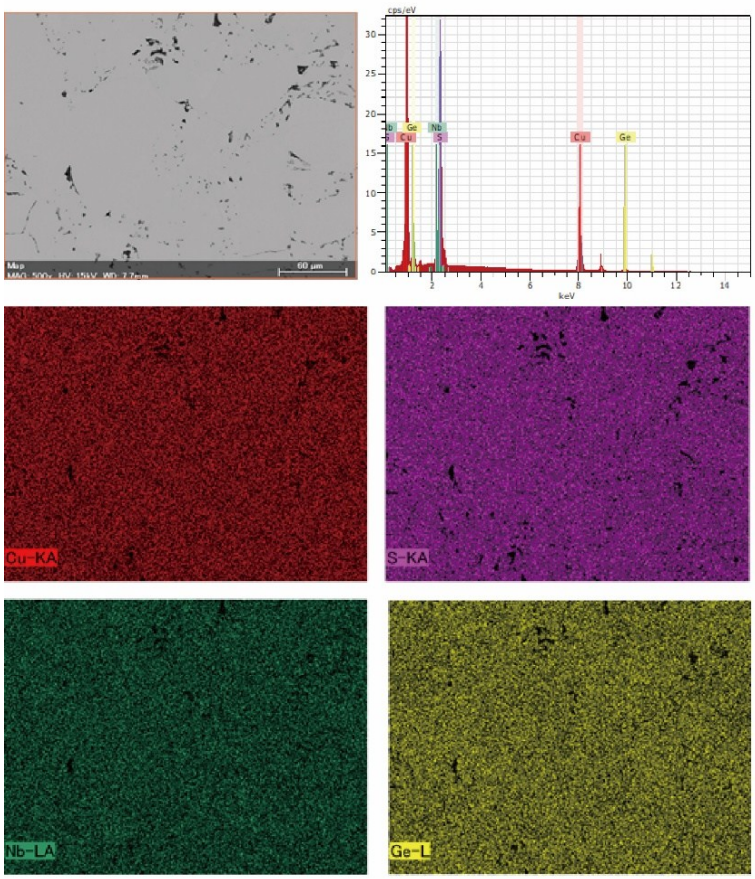

Figure S8

Scanning electron microscopy-backscattered electron microscopy image and corresponding X-ray maps of the sintered compact of $Cu_{26}Nb_2Ge_6S_{32}$.

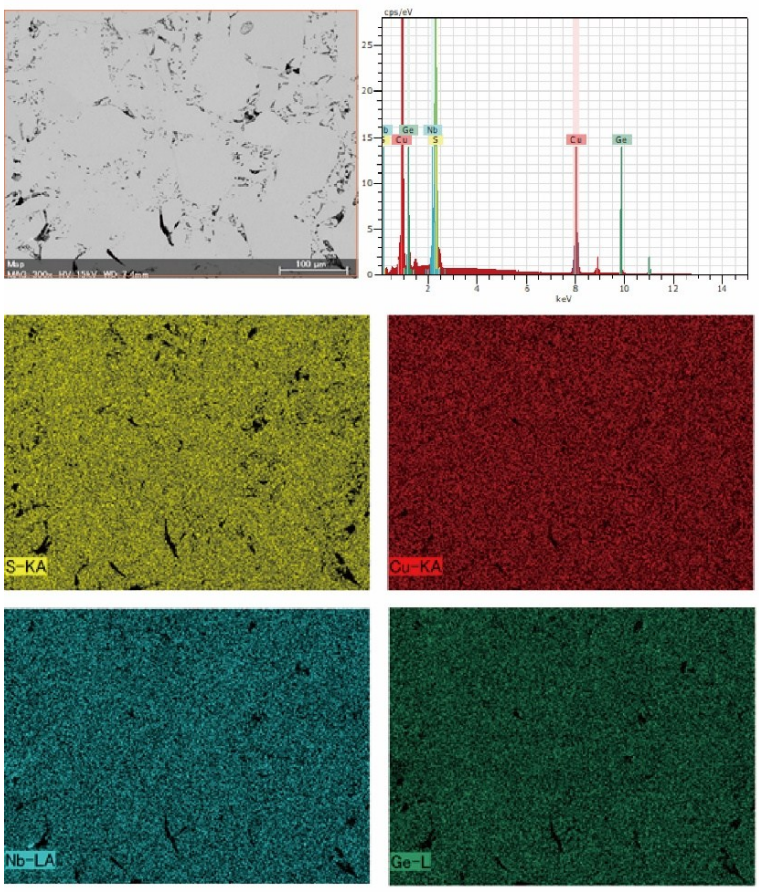

Figure S9

Scanning electron microscopy-backscattered electron microscopy image and corresponding X-ray maps of the sintered compact of $Cu_{26.3}Nb_2Ge_{5.7}S_{32}$.

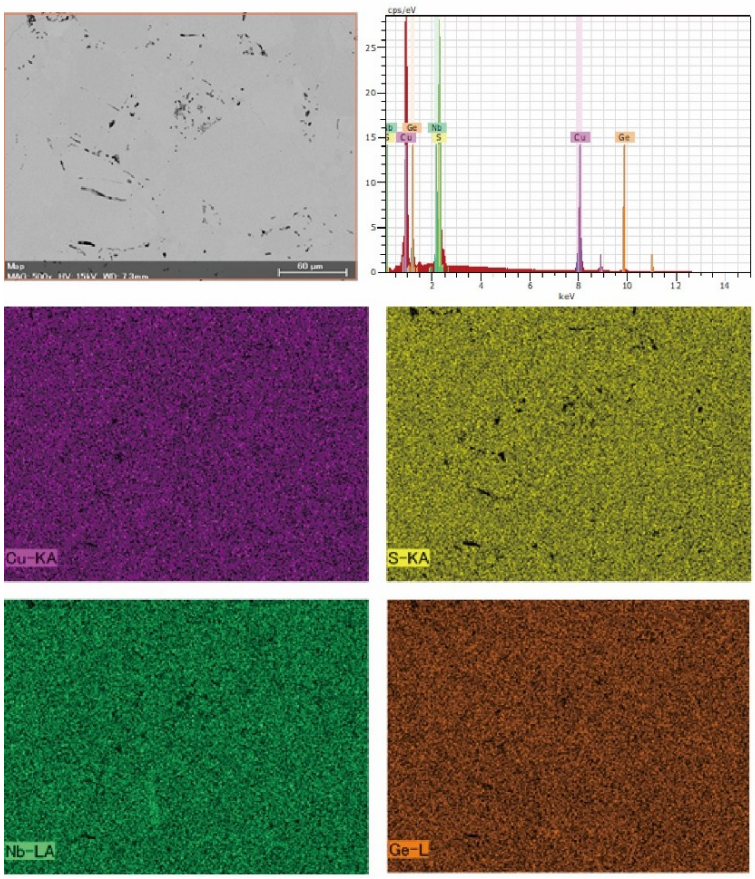

Figure S10

Scanning electron microscopy-backscattered electron microscopy image and corresponding X-ray maps of the sintered compact of $Cu_{26.5}Nb_2Ge_{5.5}S_{32}$.

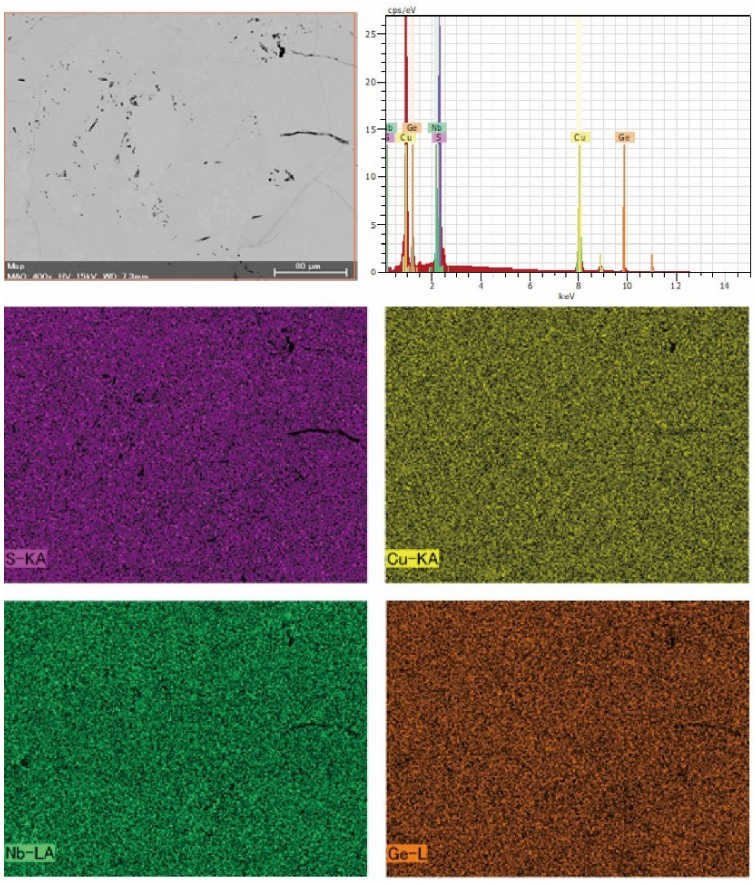

Figure S11

Scanning electron microscopy-backscattered electron microscopy image and corresponding X-ray maps of the sintered compact of $Cu_{26.7}Nb_2Ge_{5.3}S_{32}$.

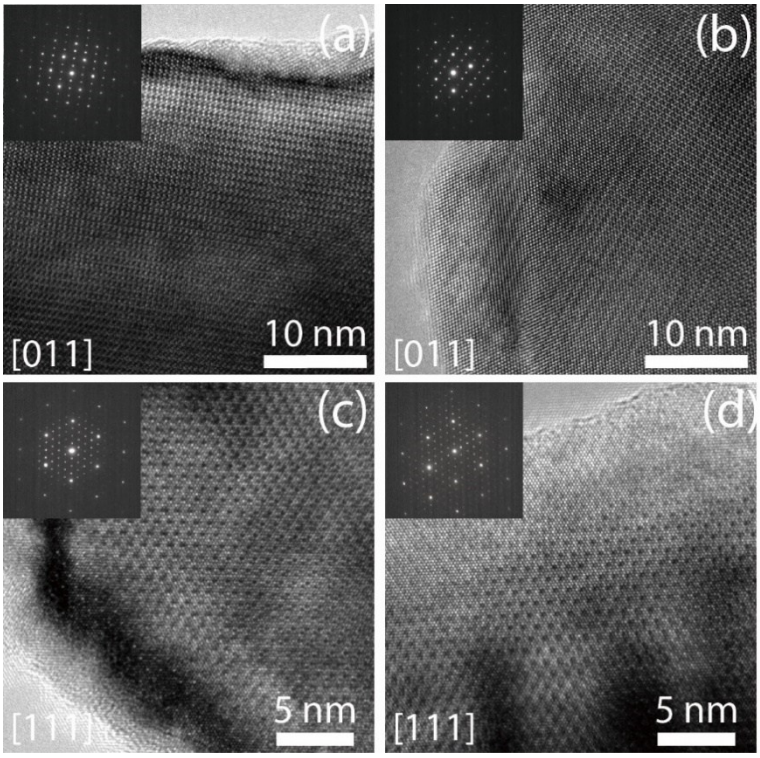

Figure S12

High-resolution transmission electron microscopy (HRTEM) images of the sintered compacts of $Cu_{26}Nb_2Ge_6S_{32}$ and $Cu_{26.5}Nb_2Ge_{5.5}S_{32}$ along the main zone axis (a),(b) [011], and (c),(d) [111], respectively. Electron diffraction patterns of the corresponding HRTEM images are given as insets.

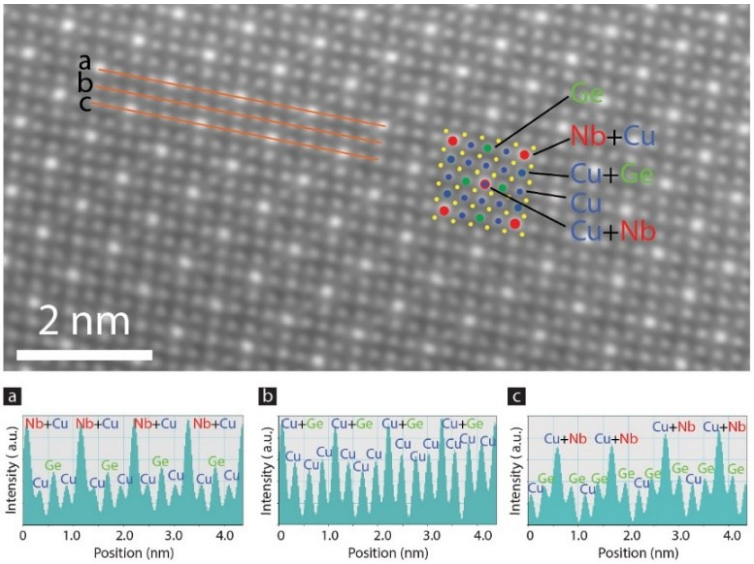

Figure S13

High-angle annular dark-field scanning transmission electron microscopy (HAADF-STEM) image of $Cu_{26}Nb_2Ge_6S_{32}$ along main zone axis [001] is shown in the top panel. The relative intensities between the columns composed of Nb+Cu, Cu+Ge, Cu, and Ge along the lines (a), (b) and (c) are shown in the bottom panel.

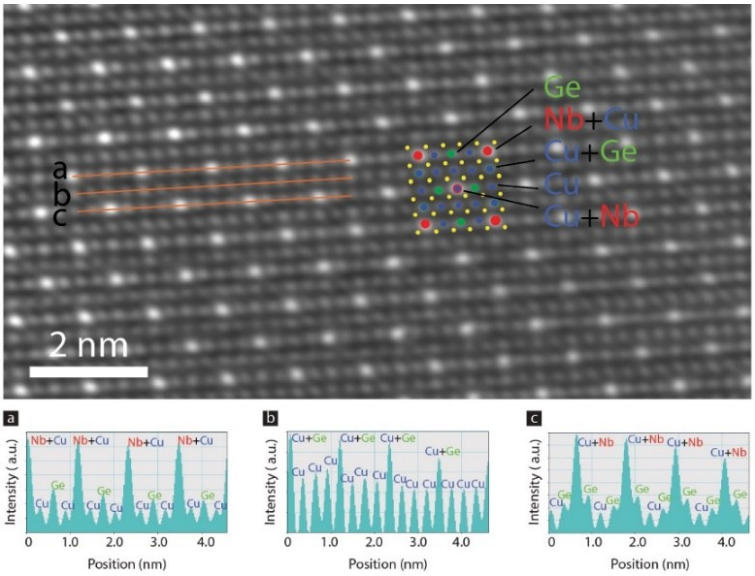

Figure S14

High-angle annular dark-field scanning transmission electron microscopy (HAADF-STEM) image of of $Cu_{26.5}Nb_2Ge_{5.5}S_{32}$ along main zone axis [001] is shown in the top panel. The relative intensities between the columns composed of Nb+Cu, Cu+Ge, Cu, and Ge along the lines (a), (b) and (c) are shown in the bottom panel.

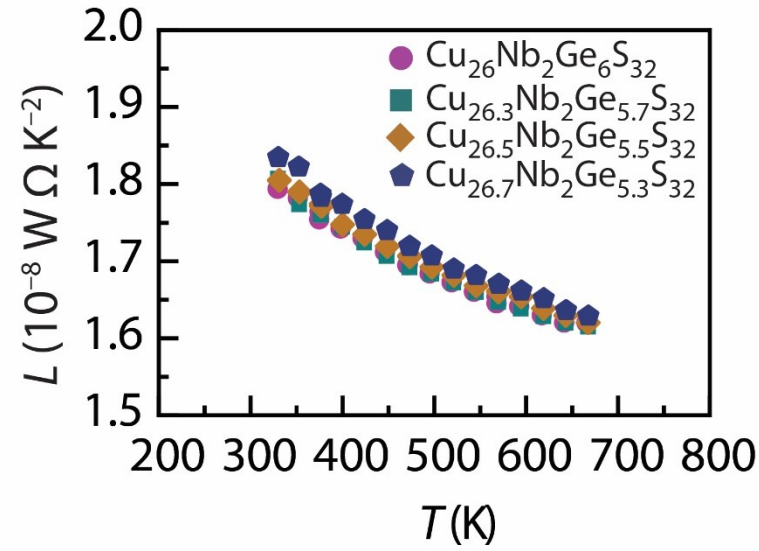

Figure S15

Temperature dependence of the estimated Lorenz number L for the sintered compacts of $Cu_{26+x}Nb_2Ge_{6-x}S_{32}$ (x = 0, 0.3, 0.5, 0.7).

Table S1

Chemical composition of the colusite matrix of the sintered compacts of $Cu_{26+x}Nb_2Ge_{6-x}S_{32}$ (x = 0, 0.3, 0.5, 0.7) determined by energy dispersive X-ray (EDX) spectroscopy of the colusite matrix. The EDX chemical compositions were averaged over fourteen spot measurements of the matrix, and normalized according to two assumptions: (i) the total content for cations (Cu, Nb, and Ge) is 34, which corresponds to the total number of crystallographic sites for cations in the unit cell, and (ii) the content for sulfur is 32. The standard deviation of the mean composition is given in parentheses.

Sample		Chemical composition			
		Cu	Nb	Ge	S
$Cu_{26}Nb_2Ge_6S_{32}$	EDX (at.%)	42.2(14)	2.8(2)	9.5(8)	45.4(13)
	(i) Cation = 34	26.3(5)	1.7(1)	5.9(5)	28.4(15)
	(ii) Sulfur = 32	29.8(13)	2.0(1)	6.7(6)	32
	Nominal	26	2	6	32
$Cu_{26.3}Nb_2Ge_{5.7}S_{32}$	EDX (at.%)	42.5(14)	2.8(2)	8.9(8)	45.8(8)
	(i) Cation = 34	26.6(5)	1.8(2)	5.6(5)	28.7(10)
	(ii) Sulfur = 32	29.7(11)	2.0(2)	6.2(6)	32
	Nominal	26.3	2	5.7	32
$Cu_{26.5}Nb_2Ge_{5.5}S_{32}$	EDX (at.%)	42.1(12)	3.3(2)	9.1(5)	45.5(10)
	(i) Cation = 34	26.3(3)	2.1(2)	5.7(3)	28.4(12)
	(ii) Sulfur = 32	29.6(11)	2.3(2)	6.4(4)	32
	Nominal	26.5	2	5.5	32
$Cu_{26.7}Nb_2Ge_{5.3}S_{32}$	EDX (at.%)	42.4(14)	3.3(2)	8.5(5)	45.8(11)
	(i) Cation = 34	26.6(5)	2.1(2)	5.3(4)	28.6(10)
	(ii) Sulfur = 32	29.6(12)	2.3(2)	5.9(4)	32
	Nominal	26.7	2	5.3	32

Table S2

Measured density d_{meas} and theoretical density d_{theo} of the sintered compacts of $Cu_{26+x}Nb_2Ge_{6-x}S_{32}$ (x = 0, 0.3, 0.5, 0.7). The d_{theo} was calculated from the estimated lattice parameter a (Table S1 in the Supplementary Information) and nominal chemical composition.

Sample	d_{meas} (g cm^{-3})	d_{theo} (g cm^{-3})
	300 K	300 K
$Cu_{26}Nb_2Ge_6S_{32}$	4.56	4.49
$Cu_{26.3}Nb_2Ge_{5.7}S_{32}$	4.62	4.47
$Cu_{26.5}Nb_2Ge_{5.5}S_{32}$	4.70	4.46
$Cu_{26.7}Nb_2Ge_{5.3}S_{32}$	4.71	4.46